Polymer Chemistry

PAPER

View Article Online
View Journal | View Issue

Cite this: *Polym. Chem.*, 2017, **8**, 769

Exploring the electrochromic properties of poly(thieno[3,2-*b*]thiophene)s decorated with electron-deficient side groups†

Shan Shao,[a] Jingjing Shi,[a] Imran Murtaza,[b,c] Panpan Xu,[a] Yaowu He,[a] Sanjay Ghosh,[d] Xiaosi Zhu,[a] Igor F. Perepichka*[d] and Hong Meng*[a,b]

Two novel thieno[3,2-*b*]thiophene (TT)/3,4-ethylenedioxythiophene (EDOT)-based compounds of 2,5-(EDOT–TT–EDOT) type bearing electron-withdrawing side groups (4-cyanophenyl or 4-pyridyl) at 3,6-positions of the TT moiety have been synthesized. Their electropolymerization leads to electroactive conjugated polymers, **P(CNPh-ETTE)** and **P(Py-ETTE)**, which possess electrochromic properties changing the color from purple to pale grey-blue or from sand brown to pale grey-green, respectively. Cyclic voltammetry and spectroelectrochemical experiments reveal that functionalization with electron-withdrawing side groups decreases the HOMO and LUMO energy levels and contracts the band gap of materials. Both new polymers demonstrated extremely short response times of 0.9–1.1 s for bleaching and 0.34–0.35 s for coloring. **P(CNPh-ETTE)** and **P(Py-ETTE)** polymers showed reasonably good contrast (16–23%) and coloration efficiency (120–190 $cm^2\ C^{-1}$) in the visible region (at the maxima of their π–π^* transitions, 540/570 nm), and high contrast and coloration efficiency in the near-infrared region (50–62% and 324–440 $cm^2\ C^{-1}$ at 1500 nm, respectively). While the stability of the pyridine-functionalized polymer, **P(Py-ETTE)**, was shown to be low (with unstable charge–discharge characteristics, presumably due to the protonation of the pyridine ring during the redox process), **P(CNPh-ETTE)** demonstrated superior electrochromic performance retaining 91–96% of its electroactivity after 2000 cycles between −0.5 and +1.0 V. DFT calculations on these and related EDOT–TT–EDOT polymers reported by us early have been presented and analyzed to understand the structure–property relationships in this class of electrochromic polymers.

Received 21st October 2016,
Accepted 12th December 2016

DOI: 10.1039/c6py01847e

www.rsc.org/polymers

Introduction

Electrochromism is defined as the phenomenon displayed by electrochromic materials that exhibit reversible and stable changes of optical properties (transmittance, reflectance and absorbance) accompanied by the phenomenon of color change when an external electrical stimulus is applied. Hitherto, electrochromic devices (ECDs) fabricated with electrochromic (EC) materials have been utilized in numerous applications such as self-darkening mirrors,[1] smart windows,[2] displays,[3] data storage devices,[4] sunglasses,[5] electrochromic fabrics,[6,7] and others. Semiconductive conjugated polymers are attractive materials for applications in organic electronic devices such as organic photovoltaic cells (OPV),[8,9] field-effect transistors (OFET),[10,11] light-emitting diodes (OLED),[12–14] sensors[15,16] and ECDs.[17,18] Compared to inorganic EC materials and small organic molecule EC materials, using conjugated polymers (CPs) as active layers in ECDs has many advantages such as low cost production, high optical contrast, fast switching speed, high coloration efficiency, good optical memory and ease in tailoring their color by structural modifications.

Thieno[3,2-*b*]thiophene (TT) regarded as a "star molecule" is widely applied in the organic electronic domain. Compared to thiophene, the fused TT moiety possesses a larger extent of conjugation to give polymers with a lower band gap and higher charge carrier mobility.[19–22] 3,4-Ethylenedioxythiophene (EDOT) is a commercially available and oxidatively polymerizable

[a]*School of Advanced Materials, Peking University Shenzhen Graduate School, Shenzhen 518055, China. E-mail: menghong@pkusz.edu.cn; Tel: +(86)-18565807998*
[b]*Key Laboratory of Flexible Electronics (KLOFE) & Institute of Advanced Materials (IAM), Jiangsu National Synergetic Innovation Center for Advanced Materials (SICAM), Nanjing Tech University (Nanjing Tech), 30 South Puzhu Road, Nanjing 211816, China*
[c]*Department of Physics, International Islamic University, Islamabad 44000, Pakistan*
[d]*School of Chemistry, Bangor University, Deiniol Road, Bangor LL57 2UW, UK. E-mail: i.perepichka@bangor.ac.uk*

†Electronic supplementary information (ESI) available: DFT calculations on oligomers and polymers with the EDOT–TT–EDOT motif; synthesis and characterization of the studied monomers and intermediates; copies of ^{1}H NMR spectra; CV, SEC and SEM data. See DOI: 10.1039/c6py01847e

donor which is polymerized to form a PEDOT polymer at relatively low applied potentials.[23,24] The band gap of PEDOT is of 1.6 eV (ref. 23) and the films of the PEDOT polymer change the color from a deep blue in the neutral state to a transmissive sky-blue in the oxidized state.[25] In 2010, Skabara *et al.* reported a compound with the EDOT–TT–EDOT motif which showed intramolecular noncovalent S···O interactions (2.87 Å) which planarized the system. The polymer electrochemically obtained from this monomer was electroactive and showed a low band gap comparable to PEDOT (1.74 eV from optical measurements and 1.53 eV from electrochemistry).[26]

Recently, our group has designed novel compounds of EDOT–TT–EDOT type, with different attachments of EDOT units to the TT core, *i.e.* at 2,5- or 3,6-positions of TT. It has been demonstrated that the polymer obtained from the conjugated 2,5-isomer had a lower band gap (1.82 eV) and showed a better EC performance compared to the 3,6-isomer (2.00 eV), in which the conjugation was interrupted at the TT moiety (see also discussion on this issue in the DFT studies section of this paper).[27] It was also shown that tetra-EDOT substituted TT monomers can be electropolymerized at either 2,5- or both 2,5- and 3,6-sites depending on the applied potentials affording the polymers with substantially different EC properties.[28] Electropolymerization of the 2,5-isomers of EDOT–TT–EDOT monomers occurs at lower potentials giving polymers with interesting EC properties. As such, our work on this class of polymers was expanded by exploiting 3,6-sites for further tuning the EC properties of polymers. Different electron donating aryl groups have been introduced as a side functionalization of the polymers resulting in materials with a band gap of *ca.* 1.8 eV and EC switching on oxidation from blue to transparent near colorless.[29] Such a type of functionalization not only affect the energy levels and the band gap of the materials to tune their color changes in ECD but can also change the morphology of materials affecting the other important characteristics of devices (charge/discharge, memory, response time and stability). However, there are no reports on EC materials based on thieno[3,2-*b*]thiophene with electron acceptor groups at the 3,6-sites, while this information would be important for deeper understanding of the structure–property relationship and the role of electronic effects in this class of materials on their EC behavior.

The donor–acceptor (D–A) concept in conjugated polymers, introduced by Havinga,[30] is now widely used in the design of novel materials for a wide range of electronic applications. It is especially efficient for reducing and fine tuning the band gap of conjugated polymers to design low band gap polymers for OPV or in OLED with tailored color emission, as well as in the design of EC materials. Apart from conventional D–A polymers with alternating donor and acceptor fragments in the polymer backbone, side group functionalization has also been used for color modification of EC materials.[31] Owing to the strong electron-withdrawing character of the pyridine ring and cyano group, pyridyl-based[32,33] or cyano-based[34] D–A structures exhibit several advantages in organic electronics, for example a lower band gap, deeper HOMO–LUMO levels and improved short-circuit currents in OPV.

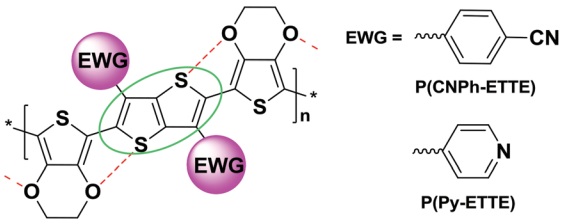

Chart 1 Novel electrochromic polymers **P(CNPh-ETTE)** and **P(Py-ETTE)** where EWG stands for the electron-withdrawing group.

In this paper, two novel polymeric materials based on EDOT–TT–EDOT repeating units decorated with electron-withdrawing 4-cyanophenyl or 4-pyridyl substituents at the positions 3,6- of the TT moiety (**P(CNPh-ETTE)** and **P(Py-ETTE**), Chart 1) have been synthesized and their EC characteristics have been studied to make a step forward in the design of EC materials with tailored properties. Particularly, we have demonstrated that while the effect of side electron-withdrawing groups toward band gap contraction is weaker than their incorporation into the main polymer chain, it is a useful approach for modification of a color palette and other properties of EC materials. Thus, the **P(CNPh-ETTE)** polymer showed improved stability and a short response time compared to its analog with a phenyl group, **P(Ph-ETTE)**. We have also supplemented our experimental results on these and previously studied EDOT–TT–EDOT polymers[27–29,35] by DFT calculations for deeper understanding the structure–property relationships in this class of EC materials.

Experimental

Materials

All starting materials were purchased from Energy Chemical, except for the $Pd(PPh_3)_4$ catalyst which was purchased from TCI. Acetonitrile (ACN), dichloromethane (DCM), chloroform ($CHCl_3$), and tetrahydrofuran (THF) were dried and distilled over calcium hydride under nitrogen. Dioxane, *N*,*N*-dimethylformamide (DMF) and toluene were dried over 4 Å molecular sieves. 3,6-Dibromothieno[3,2-*b*]thiophene (**1**)[36] and 2-tributylstannyl-3,4-ethylenedioxythiophene (**5**)[37] were synthesized according to the literature procedures.

Instruments

^{1}H NMR measurements were carried out on a Bruker Advance III nuclear magnetic resonance spectrometer operating at 400 MHz in deuterochloroform ($CDCl_3$). Mass spectra were obtained on an HRMS Thermo Q-Exactive mass spectrometer. Electron absorption UV-Vis-NIR spectra of the polymeric films were obtained on a Lambda 750 spectrophotometer. Electrochemical studies were carried out using a CHI620E electrochemical workstation. The thickness of polymeric films was measured with a VK-X200 3D laser scanning confocal

microscope. Atomic force microscopy (AFM) images were obtained on a MultiMode 8 Bruker AFM using the tapping mode. Scanning electron microscopy (SEM) images were obtained on a Carl Zeiss SUPRA® 55 SEM instrument.

Electrochemistry and spectroelectrochemistry

Electrochemical experiments (electropolymerization, cyclic voltammetry (CV) of monomers and polymers, and chronoamperometry) were performed in a standard three-electrode cell scheme using a silver wire as the pseudo-reference electrode, a platinum wire as the counter electrode and an ITO-coated glass slide or a Pt disk (d = 2 mm) as the working electrode. Electropolymerization of the monomers (**Py-ETTE** or **CNPh-ETTE**, 0.6 mM solutions) was performed in anhydrous solvents (DCM/THF, 60/40 v/v for **CNPh-ETTE** or $CHCl_3$/ACN, 75/25 v/v for **Py-ETTE**) with 0.1 M tetrabutylammonium hexafluorophosphate ($TBAPF_6$) as the supporting electrolyte at a scan rate of 100 mV s^{-1} for 20 cycles under ambient conditions. Under the repetitive CV cycling between the potentials of the neutral (*ca.* −0.8 to +0.2 V) and oxidized states (*ca.* +1.2 V) of the monomers, the colored polymer films were electrodeposited on the Pt disk electrode. Cyclic voltammograms of the polymer films were obtained using the same electrode setup in the monomer-free ACN solution containing 0.1 M $TBAPF_6$ under a nitrogen atmosphere. For spectroelectrochemical experiments (SEC), the polymer films were electrodeposited in the same fashion on an ITO-coated glass electrode and their UV-Vis-NIR spectra at different applied potentials were recorded. The potentials were calibrated *versus* the ferrocene/ferrocenium redox pair (Fc/Fc^+) as an internal standard, which showed the half-wave potential $E_{1/2}$ = +0.52 V *versus* the Ag wire pseudo-reference electrode in ACN/$TBAPF_6$ (0.1 M) at 100 mV s^{-1} (Fig. S18, ESI†). The coloration efficiency (CE) was estimated as a ratio of a change in the optical density of the polymer film between the neutral and doped (colored and bleached) states [$\Delta OD = OD_{red} - OD_{ox} = \log(T_{ox}/T_{red})$] and the amount of injected/ejected charges per unit area (C cm^{-2}) ($Q_d = Q/A$, A is an area of the polymer film) at a given wavelength: $CE = \Delta OD/Q_d$. Here OD and T are optical densities and transmittances, respectively; subscripts "red" and "ox" denote neutral (colored) and oxidized (bleached) states.

Computational methodology

Computational studies were carried out using density functional theory (DFT) with the Gaussian 09 [38] package of programs. The geometries were fully optimized for isolated molecules in the gas phase, with no constraints unless otherwise stated (see ESI†). Becke's three-parameter hybrid exchange functional[39] with the Lee–Yang–Parr gradient-corrected correlation functional (B3LYP)[40] and Pople's 6-31G split valence basis set supplemented by d-polarization functions for heavy atoms were employed. The restricted Hartree–Fock formalism was used. The electronic structures of B3LYP/6-31G(d) optimized geometries were calculated at the same level of theory. The molecular orbital density plots have been prepared with GaussView software v5.0.8 at 0.015 isovalues for the surfaces. Optimization of the geometries of the polymers and calculation of their electronic structures were performed using the periodic boundary conditions formalism (PBC) at the PBC/B3LYP/6-31G(d) level, which generally gives a good estimate of the band gaps of conjugated polymers, including polythiophenes.[41–43] The PBC calculated HOCO/LUCO energies (highest occupied/lowest unoccupied crystal orbitals) and the band gaps (E_g) were compared with the results based on the oligomers approach of extrapolations of HOMO/LUMO energies (highest occupied/lowest unoccupied molecular orbitals) to the infinite length chain showing good coincidence.

Results and discussion

DFT studies

To understand the structural effect in the polymers with the EDOT–TT–EDOT motif, particularly the effect of 3,6-substituents R in 2,5-bis(EDOT)–TT polymers **P(R-ETTE)** (Chart 2) on their geometries, HOMO/LUMO energy levels and the band gaps, we have performed DFT calculations for the corresponding oligomers (with n = 1–6; up to n = 10 in some cases) at the B3LYP/6-31G(d) level. The data on the chain length dependences were extrapolated to infinite number of monomer units in the chain ($n = \infty$) and the results were compared with calculations of the corresponding polymers by the PBC formalism at the same level of theory.

Unsubstituted **(H-ETTE)$_n$** oligomers adopt planar structures due to attractive non-covalent S···O interactions in both EDOT–EDOT and TT–EDOT fragments of the molecules which

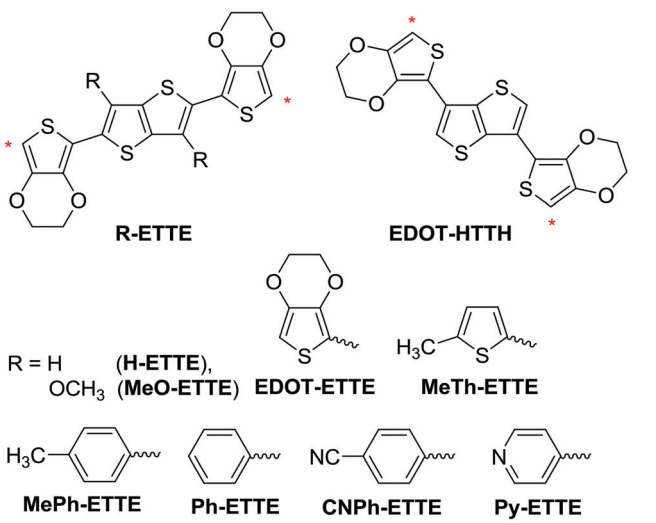

Chart 2 Structures of monomers, oligomers and polymers with the EDOT–TT–EDOT motif studied by DFT. Asterisks show the places of connections for oligomers and polymers. In the text, acronyms **(R-ETTE)$_n$/P(R-ETTE)** and **(EDOT-HTTE)$_n$/P(EDOT-HTTH)** are used for the corresponding oligomers and polymers. Calculations for **MeTh-ETTE** and **MePh-ETTE** with methyl groups were done to model the corresponding polymers with hexyl substituents recently studied in ref. 29.

act to enforce the planarity (see Fig. 1a and S1a in the ESI† for hexamer). For the optimized structures, the interatomic S···O distances in both fragments are significantly shorter than the sum of van der Waals radii for sulphur and oxygen (1.80 + 1.52 = 3.32 Å) and are in the range of 2.94–2.96 Å, which is close to the single crystal X-ray diffraction data for short S···O contacts in the **R-ETTE** monomer with R = $C_{16}H_{33}$ (2.87 Å),[26] in EDOT–EDOT (2.91–2.93 Å)[44] and EDOT–thiophene oligomers (2.96, 3.02).[45] This leads to a very planar structure of the main chain: for longer oligomers, the dihedral angles between the TT and EDOT moieties are very small (1–3° for the hexamer and 0.5–1.5° for the decamer). The HOMO and LUMO orbital energies and the HOMO–LUMO gap (ΔE_{HL}) show a typical asymptotic dependence on the length chain with saturation at $n \sim 10$ (Fig. 2). As commonly observed for conjugated oligomers,[46] plots *versus* the reciprocal number of the chain length, $1/n$, are linear for shorter oligomers but tend to deviate from linearity and to saturate for $n > 6$ (Fig. S6 and S7, ESI†). We have found that they correlate linearly with the empirical parameter $1/n^{1.5}$ and the extrapolated values to $n = \infty$ excellently coincide with HOCO and LUCO energies and the band gaps (E_g) for the polymer **P(H-ETTE)** (Fig. 2).[47]

Similar planar conformations were found for the optimized geometries of **(MeO-ETTE)$_n$** oligomers (see Fig. S1b in the ESI† for hexamer), in which case short S···O distances of 2.94–2.96 Å were also found (including S···OMe contacts), although the dihedral angles between the TT and EDOT moieties were slightly larger (3–5° for the hexamer). Compared to **(H-ETTE)$_n$** oligomers, in its isomer with the 3,6-linkage of EDOT to the TT moiety, **(EDOT-HTTH)$_n$**, the increased steric repulsions between the TT and EDOT rings led to an increased dihedral angle of ~14–16°. Therefore, depending on the signs of the two dihedral angles at the EDOT–TT–EDOT fragment, the oligomers adopted different conformations: twisted conformation to form a helix in the case of the same signs of the dihedrals and planar conformation in the case of the opposite signs of the dihedrals (Fig. 1b and S2 in the ESI†). The helix conformation was found to be of lower energy by 5.0 kJ mol^{-1}.

An introduction of 3,6-substituents sterically disturbed the main chain of **(R-ETTE)$_n$** oligomers leading to increased dihedral angles in the EDOT–TT–EDOT fragments (Table S1 and Fig. S9 in the ESI†). Here again, depending on the sign of the rotation at both the sides of the TT moiety, the oligomers adopted helix or planar conformations (Fig. 1c, d and S3–S5 in the ESI†). Therefore, calculations have been performed for both conformers to compare their stabilities. In most cases, the helix conformation was found to be more stable than the planar one (by 15.4–16.7 kJ mol^{-1} for hexamers with R = Ph, CNPh and Py, and by 3.2 kJ mol^{-1} for R = MeTh). For **(EDOT-ETTE)$_n$**, planar conformations were found to be more stable (by 3.0 kJ mol^{-1} for hexamer). In the helix conformations of **(R-ETTE)$_n$**, the EDOT–TT dihedral angles in the backbone were found to be ~19–26° (for hexamers) in the case of R = MePh, Ph, CNPh and Py and somewhat lower (~6–14°)

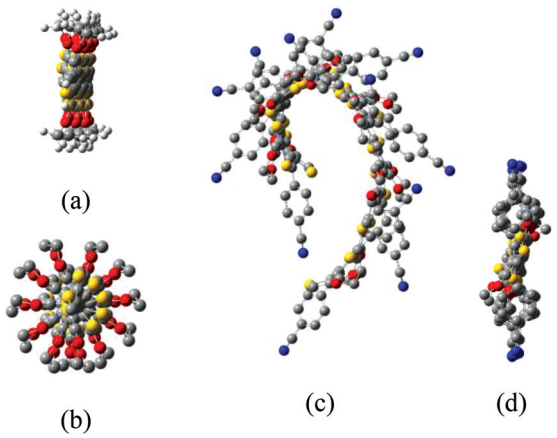

Fig. 1 B3LYP/6-31G(d) optimized geometries of hexamers: (a) **(H-ETTE)$_6$**, (b) helix conformation of **(EDOT-HTTH)$_6$**, (c, d) helix and planar conformations of **(CNPh-ETTE)$_6$**. Views along the oligomer chains are shown; hydrogen atoms in (b–d) are omitted for clarity.

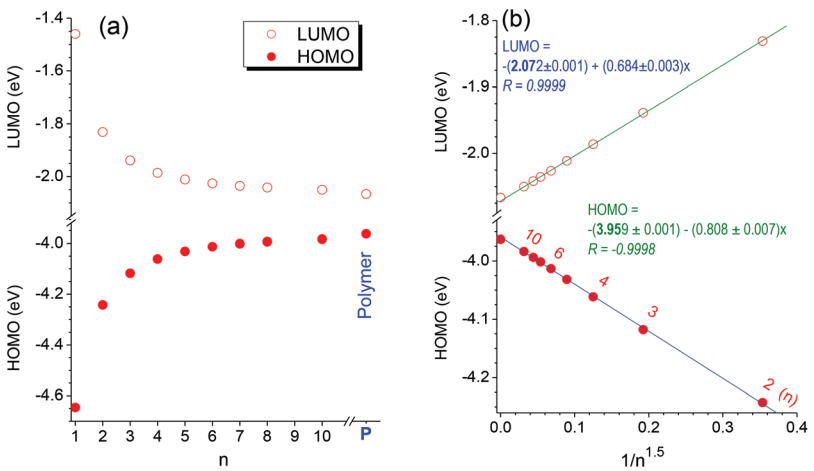

Fig. 2 Chain length dependences of HOMO and LUMO energies for B3LYP/6-31G(d) optimized geometries of **(H-ETTE)$_n$** oligomers and for **P(H-ETTE)** (by PBC). The lines correspond to linear fitting of the energies *vs.* $1/n^{1.5}$.

for R = EDOT and MeTh. Large dihedral angles between the side R groups and the TT moiety (52–58° for R = MePh, Ph, CNPh, Py and 61–71° for R = EDOT and MeTh) indicate that they are relatively weakly conjugated to the main chain of the oligomers (and polymers). Also, planar conformations showed somewhat lower EDOT–TT dihedral angles in the backbone and larger dihedral angles between the TT moiety and the side R groups (Table S1 and Fig. S9 in the ESI†).

In the case of thiophene-substituted oligomers **(R-ETTE)$_n$** (R = EDOT and MeTh), the HOMO and LUMO energy levels for both conformations are almost the same. For R = Ph, CNPh and Py, the difference in energy levels between the helix and planar conformations became larger: the helix conformations showed lower both HOMO and LUMO, and slightly larger HOMO–LUMO energy gaps compared to the corresponding planar conformations (Fig. 3). The largest differences were observed for **(CNPh-ETTE)$_n$** oligomers. Thus, for the hexamer **(CNPh-ETTE)$_6$** these differences between the helix and planar conformations were found to be −0.13 eV, −0.06 eV and +0.06 eV for HOMO, LUMO and ΔE_{HL}, correspondingly (Fig. 3, Table S1 and Fig. S9 in the ESI†).

Similarly to unsubstituted oligomers **(H-ETTE)$_n$**, with an increase of the chain length of oligomers **(R-ETTE)$_n$**, an asymptotic increase of the HOMO and a decrease of the LUMO were observed *versus* n for both helix and planar conformations, with nice linear correlations (R = 0.996–0.9999) *versus* $1/n^{1.5}$ (Fig. 3). For planar conformations, these linear plots extrapolated to $n = \infty$ excellently coincided with the HOCO and LUCO energies calculated for polymers by the PBC approach, whereas extrapolated (to $n = \infty$) HOMO and LUMO energies for helix conformations gave somewhat lower energies (by 0.05–0.12 eV and 0.03–0.08 eV, respectively) (Fig. 3; for other oligomers and polymers see Tables S2, S3 and Fig. S6–S8 in the ESI†).

Considering that the HOMO and LUMO energy levels of the oligomers became close to saturation at $n \sim 6$ (Fig. 2 and 3), the hexamers **(R-ETTE)$_6$** and **(EDOT-HTTH)$_6$** represent sufficiently long conjugated structures to model the localization of frontier orbitals in the corresponding polymers. Fig. 4 shows the HOMO and LUMO orbital densities in **(H-ETTE)$_6$** and **(CNPh-ETTE)$_6$** hexamers. Distribution of both HOMO and LUMO orbital densities in planar conformation of **(CNPh-ETTE)$_6$** is very similar to the unsubstituted hexamer **(H-ETTE)$_6$** with delocalization along the main chain and with

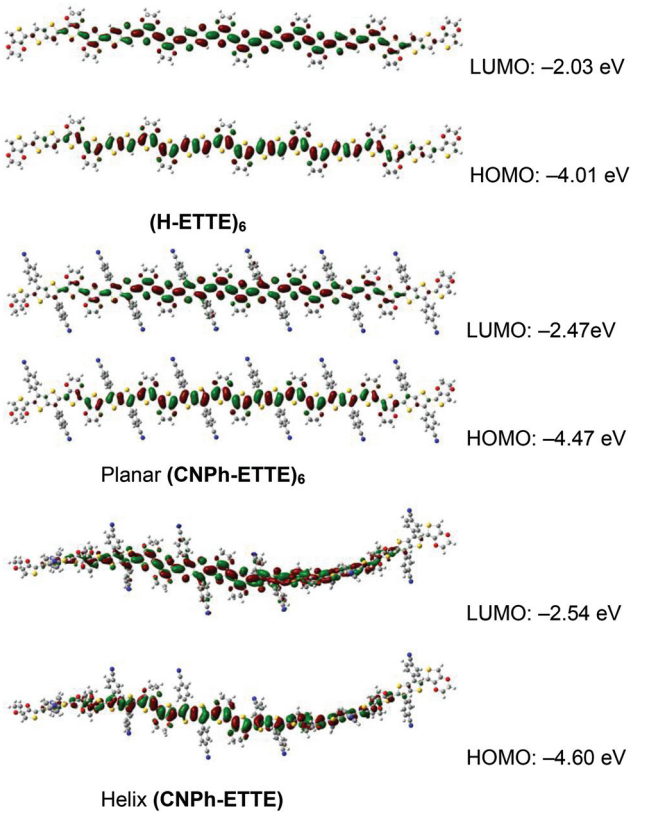

Fig. 4 HOMO and LUMO energies and orbital coefficients for **(H-ETTE)$_6$** and **(CNPh-ETTE)$_6$** (in both the helix and the planar conformations) from B3LYP/6-31G(d) calculations. For other hexamers, see Fig. S9 in the ESI.†

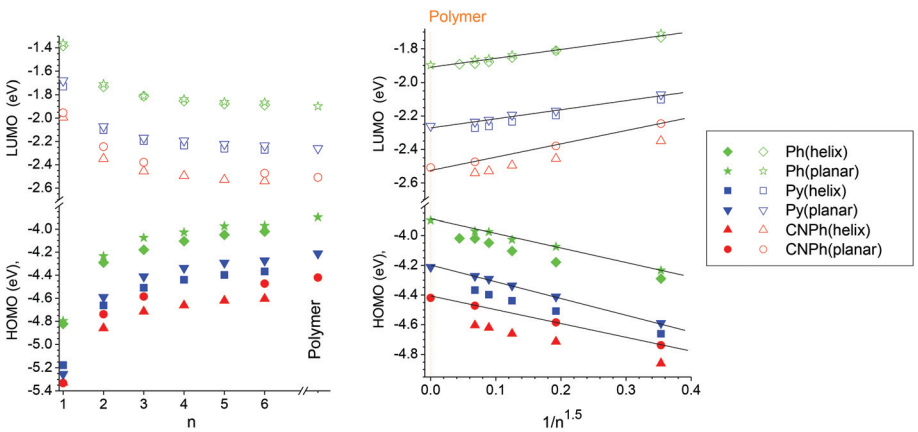

Fig. 3 Chain length dependences of HOMO and LUMO energies for B3LYP/6-31G(d) optimized geometries of helix and planar conformations of **(R-ETTE)$_n$** oligomers (R = Ph, CNPh, Py) for corresponding polymers **P(R-ETTE)** (by PBC). The lines correspond to linear fitting of energies *vs.* $1/n^{1.5}$.

higher orbital densities in the middle part of the molecules. The helix conformation of **(CNPh-ETTE)$_6$**, which is energetically preferential, shows the same fashion and degree of delocalization of the HOMO and LUMO orbitals on the π-system of the backbone. Almost no frontier orbital coefficients were observed on the side 4-cyanophenyl groups in **(CNPh-ETTE)$_6$**. Thus, the electron-withdrawing 4-cyanophenyl side groups electronically affect the frontier orbital energy levels, decreasing both LUMO and HOMO orbital energies, but do not participate in the orbital delocalization. The effect on the LUMO is somewhat larger than on the HOMO resulting in some energy gap contraction in **(CNPh-ETTE)$_6$** compared to its analog **(Ph-ETTE)$_6$** (by 0.07 eV and 0.11 eV, for helix and planar conformations, respectively; Table S1, ESI†). Similar orbitals density distribution is observed for other **(R-ETTE)$_6$** oligomers where highly distorted side groups are not involved in HOMO/LUMO delocalization (Fig. S9, ESI†). In the case of **(EDOT-HTTH)$_6$** with the 3,6-linkage of the main chain, the distribution of HOMO and LUMO orbital densities is differently clear showing an interruption of the conjugation at the TT unit, with no HOMO/LUMO coefficients at the central C=C atoms of the TT moiety and, accordingly, substantially lower HOMO and higher LUMO energy levels for these oligomers compared to others (Fig. S9 and S10, ESI†).

Fig. 5 summarizes the results on variations in frontier orbital energy levels for structures shown in Chart 2, from monomers (HOMO, LUMO) to polymers (HOCO, LUCO) (see also Fig. S11 and Table S2 in the ESI†). The electron donating MeO group and thiophene substituents (EDOT, MeTh) increase the HOCO energies of polymers by 0.1–0.14 eV, but have a weaker effect on the band gaps, which are in the range of 1.90–1.93 eV. As expected, the Ph group has a smaller effect on the HOCO but give a somewhat wider band gap for polymer **P(Ph-ETTE)** of 2.00 eV. An introduction of electron withdrawing CNPh and Py substituents substantially decreases both the HOCO and LUCO energy levels and leads to some band gap contraction due to a somewhat higher effect on the LUCO than on the HOCO energy levels (1.91 eV for **P(CNPh-ETTE)**). It should be noted that because computations have been performed in the gas phase, the results characterize the electronic states of the isolated chains of the oligomeric/polymeric molecules. The solid state effects, intermolecular interactions and morphology of the experimentally studied polymers might additionally affect the properties of materials.

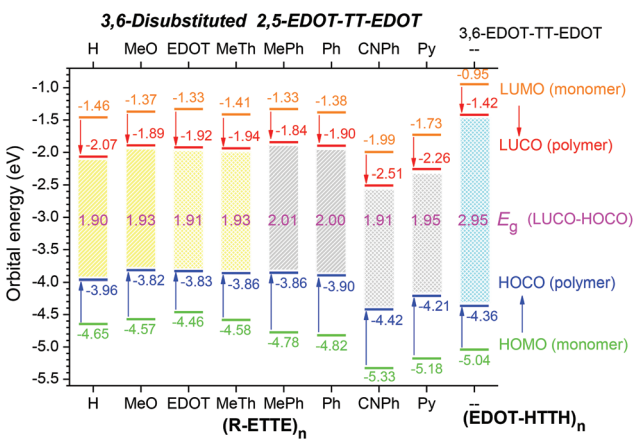

Fig. 5 Evolution of the frontier orbital energy levels from monomers (HOMO, LUMO) to polymers (HOCO, LUCO) and the band gaps of different polymers at B3LYP/6-31G(d) optimized geometries (by PBC for polymers).

The structural isomer of **P(H-ETTE)** with the 3,6-linkage in the main polymer chain, *i.e.* **P(EDOT-HTTH)**, shows lower HOCO (by 0.4 eV) and higher LUCO (by 0.65 eV) resulting in substantially larger (by 1.05 eV) E_g = 2.95 eV (Fig. 5). The reason for that is an interrupted conjugation at the TT moiety along the backbone as clearly seen from the HOMO/LUMO orbital distribution in the hexamer **(EDOT-HTTH)$_6$** (Fig. S9, ESI†). There are no HOMO or LUMO orbital densities on the central C=C π-bond of the TT moiety and the delocalization of the π-orbitals along the main chain is limited by two EDOTs and two halves of neighboring TT units. Experimentally found values for the electrochemically prepared polymers from **EDOT-HTTH** and **H-ETTE** monomers gave a substantially smaller difference in their band gap of 0.18 eV only (E_g = 2.00 eV and 1.82 eV, respectively).[27] This might indicate that the electropolymerization of **EDOT-HTTH** occurred not only at the EDOT sites but (partly) at the 2,5-CH of the TT unit extending the conjugation length of the resulting material.

Monomer synthesis

The synthetic route to the target monomers is depicted in Scheme 1. Synthesis of the monomer **Ph-ETTE** by this scheme was recently reported by us.[29] We have applied this route to the monomers **CNPh-ETTE** and **Py-ETTE** with electron-withdrawing groups. Suzuki coupling of 3,6-dibromothieno[3,2-*b*]thiophenes (**1**)[36] with 4-cyanophenyl- or 4-pyridylboronic acids did not work well in DMF or toluene (in contrast to the synthesis of **2a**), but the reflux in dioxane with Pd(PPh$_3$)$_4$ as the catalyst gave us the desired compounds **2b,c**. Bromination of **2a** (and its analogs with 4-hexylphenyl and 5-hexyl-thienyl groups) with *N*-bromosuccinimide (NBS) proceeded smoothly in a chloroform–acetic acid mixture at room temperature to give **3a** with a high yield of 95%.[29] Electron-withdrawing substituents at position 3,6-substantially decrease the reactivity of the TT moiety and bromination required overnight heating (at 100 °C or at reflux) in DMF to obtain compounds **3b,c** in moderate yields of 60–74%. Their Stille coupling with 2-tributylstannyl-EDOT (**5**) resulted in the target monomers **CNPh-ETTE** and **Py-ETTE** as a greenish-yellow and light yellow solid, respectively. Both monomers have poor solubility in common organic solvents (**Py-EDOT** < **PhCN-EDOT** ~ 2 mM in DCM).

Electrochemical polymerization

The oxidative electropolymerization of monomers **CNPh-ETTE** and **Py-ETTE** (~0.6 mM concentration) was carried out under potentiodynamic conditions in a mixed solvent (DCM/THF, 60/40 v/v for **CNPh-EDOT** and CHCl$_3$/ACN, 75/25 v/v for **Py-EDOT**) containing 0.1 M TBAPF$_6$ as the supporting electrolyte.

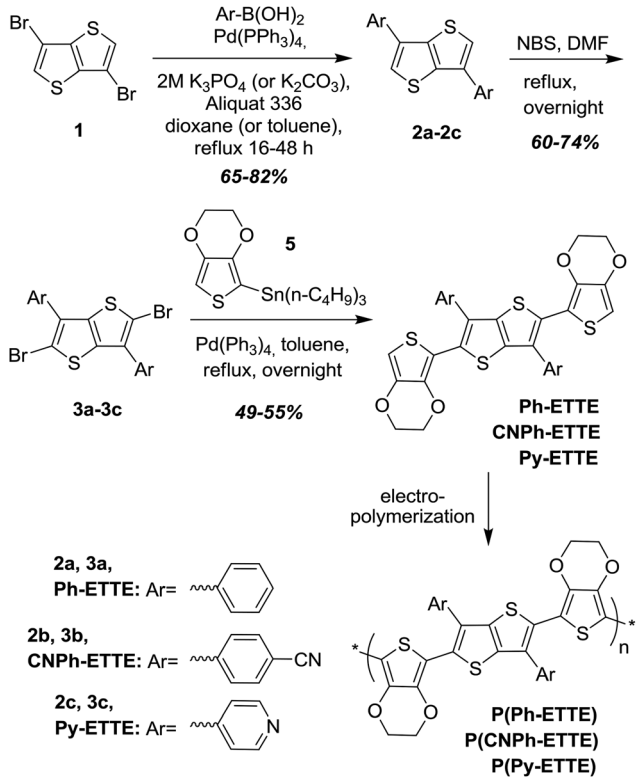

Scheme 1 Synthesis of monomers **Ar-ETTE** and their electropolymerization to **P(Ar-ETTE)**.

Due to the presence of electron-withdrawing groups, their oxidation appeared at higher potentials (E^{ox}_{pa} = 0.83 V and 1.11 V, E^{ox}_{onset} = 0.92 V and 0.80 V, for **CNPh-ETTE** and **Py-ETTE**, respectively) compared to **Ph-ETTE** (E^{ox}_{pa} = 0.80 V, E^{ox}_{onset} = 0.69 V (ref. 29)).

Repetitive cyclic voltammetry (CV) scanning between −0.8 V and 1.2 V (for **CNPh-ETTE**) or between −0.2 and 1.2 V (for **Py-ETTE**) resulted in progressive growth of the new CV waves at lower potentials than oxidation potentials of the monomers indicating the growth of the electroactive polymer films on the Pt electrode surface (Fig. 6a and b).

After electrochemical polymerization, the deposited polymer films were rinsed with ACN to remove the monomers and the electrolyte and their electrochemical response was tested by CV in ACN/$TBAPF_6$ (0.1 M) for both p- and n-doping processes (Fig. 6c and d). Polymer **P(CNPh-ETTE)** films showed reversible p-doping with two well-defined reversible redox couples at E^{ox}_{pa}/E^{ox}_{pc} = 0.43/0.28 V and 0.83/0.80 V *versus* the Ag wire pseudo-reference electrode, which can be attributed to the formation of polaron and bipolaron charge carriers.[6] Its onset oxidation potential of E^{ox}_{onset} = 0.09 V is only slightly higher than that of **P(Ph-ETTE)** (0.07 V).[29] Apparently, the **P(Py-ETTE)** films showed p-doping at substantially higher potentials with an onset of E^{ox}_{onset} = 0.83 V (one reversible wave with E^{ox}_{pa}/E^{ox}_{pc} = 1.11/1.04 V). This unexpected result cannot be explained by the electron-withdrawing character of the 4-pyridyl substituent, which is a weaker accepting group compared to the 4-cyanophenyl group (compare the HOMO of **CNPh-ETTE** and **Py-ETTE** monomers and polymers in Fig. 5).

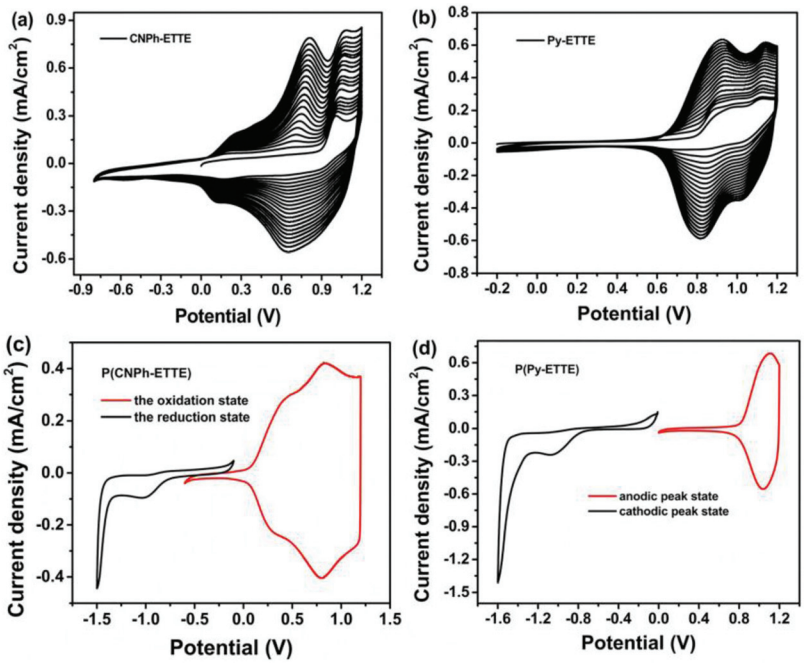

Fig. 6 Potentiodynamic electrochemical polymerization of 0.6 mM monomers: (a) **CNPh-ETTE** (DCM/THF, 60/40, v/v) and (b) **Py-ETTE** ($CHCl_3$/ACN, 75/25, v/v) with $TBAPF_6$ (0.1 M) on the Pt disk electrode at 100 mV s^{-1} (20 cycles are shown). Cyclic voltammograms of electrodeposited polymer films on the Pt disk electrode in a monomer-free ACN/$TBAPF_6$ (0.1 M) solution at 100 mV s^{-1} under a nitrogen atmosphere: (c) **P(CNPh-ETTE)** and (d) **P(Py-ETTE)**. Potentials are *vs.* Ag wire.

We rationalize this observation as partial protonation of pyridine rings in **P(Py-ETTE)** during the electropolymerization process. Oxidative coupling of the monomer units during electropolymerization results in the formation of protons. Pyridine groups present in the monomer **Py-ETTE** and polymer **P(Py-ETTE)** can partially trap these protons before they are reduced at the counter electrode. So, such partial protonation of the pyridine groups might decrease the HOMO energy level of the resulting polymer, as well the degree of polymerization and the quality of the polymer films. To check this hypothesis, we treated the **P(Py-ETTE)** film with hydrazine hydrate to deprotonate/dedope the polymer. This treatment resulted in a pronounced cathodic shift of the **P(Py-ETTE)** oxidation potential to E^{ox}_{onset} = 0.53 V in the first CV cycle, which, however, returned back to its original value of +0.81 V on further cycling (Fig. S19, ESI†). This might indicate that initially the deprotonated/dedoped polymer film undergoes (partial) protonation during anodic cycling, perhaps, by protons formed by an oxidation of traces of water[48] to be present in the film (or in the solvent). Thiophene–pyridine copolymers with a pyridine ring in the main chain have been previously studied,[49–51] and it was shown that the pyridine ring is sufficiently basic to be protonated.[51] Such protonation, however, was not observed when the pyridine ring is inserted in the polymer backbone as a chalcogenodiazolo[3,4-*c*]pyridine moiety, in which case the basicity of a pyridine ring is substantially decreased, so the polymer is not protonated on electropolymerization or on cycling.[52,53]

Both **P(CNPh-ETTE)** and **P(Py-ETTE)** polymers showed irreversible n-doping in cathodic scans with onset reduction potentials of −1.37 V and −1.49 V, respectively (Fig. 6c, d and S20 in the ESI†).[54] The difference between the reduction potentials of **P(CNPh-ETTE)** and **P(Py-ETTE)** of 0.12 V is in reasonable agreement with the difference in their LUMO energy levels from DFT (0.25 eV, Fig. 5). Irreversible reduction peaks were decreased gradually on cycling indicating the instability of the polymers toward n-doping, presumably due to the high reactivity of the reduced forms of the polymers[49] which are degraded by traces of oxygen and/or water.[48]

Cyclic voltammograms of electrodeposited polymer films at different scan rates (from 50 to 500 mV s^{-1}) are shown in Fig. 7a and b. The anodic (j_{pa}) and cathodic (j_{pc}) peak current densities for the p-doping/dedoping processes showed excellent linear dependences ($R \geq 0.999$) *versus* the potential scan rate indicating that both the redox processes are non-diffusional and the polymeric films are well adhered to the Pt electrode surface (Fig. 7c and d).

Also, the amounts of charge and discharge remain constant even at high scan rates, confirming the good charging and discharging (doping/dedoping) ability of the polymers.[55] Moreover, the calculated ratios of anodic/cathodic peak current densities (j_{pa}/j_{pc} = 1.04 for **P(CNPh-ETTE)** and 1.27 for **P(Py-ETTE)**, Fig. 7) were smaller than that observed for **P(Ph-ETTE)** films (j_{pa}/j_{pc} = 1.36).[29] For **P(CNPh-ETTE)**, j_{pa}/j_{pc} is very close to 1, indicating its excellent reversibility during p-doping/dedoping, which was confirmed by the stability test (see below). Surprisingly **P(Py-ETTE)** showed relatively good reversibility of p-doping/dedoping (as follows from the linear dependences of j_{pa} and j_{pc} *vs.* the scan rate and its j_{pa}/j_{pc} ratio, Fig. 7b and d), although longer stability tests indicated its degradation (discussed below).

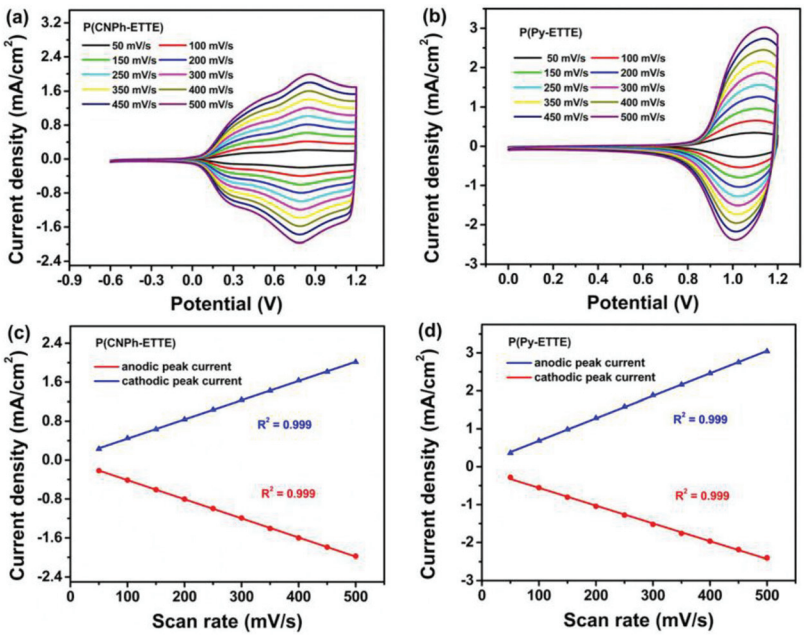

Fig. 7 Cyclic voltammograms (a, b) and scan rate dependences of current densities at peak currents (b, d) of polymeric films on the Pt disk electrode in a monomer-free ACN/$TBAPF_6$ (0.1 M) solution at different scan rates from 50 to 100, 150, 200, 250, 300, 350, 400, 450 and 500 mV s^{-1}: (a, c) **P(CNPh-ETTE)** from −0.6 to 1.2 V; (b, d) **P(Py-ETTE)** from 0 to 1.2 V.

Spectroelectrochemistry and colorimetry

The spectroelectrochemical experiments (SEC) were carried out to explore the optical changes of the polymer films on p-doping. The films of **P(CNPh-ETTE)** and **P(Py-ETTE)** were electrodeposited potentiodynamically (20 cycles) from their monomer solutions on indium tin oxide (ITO) coated glass slides under the same conditions as described above for CV studies (Fig. S21, ESI†). The thicknesses of the films measured by laser scanning confocal microscopy were 100 nm for **P(CNPh-ETTE)** and 105 nm for **P(Py-ETTE)**.

Fig. 8 shows the SEC properties of the polymers and the corresponding colors of the films. In their neutral forms, polymers **P(CNPh-ETTE)** and **P(Py-ETTE)** showed broad structureless π–π^* transition absorption bands peaked at 580 nm and 545 nm, respectively. Compared to these polymers with electron-withdrawing 3,6-substituents, the **P(Ph-ETTE)** polymer in its neutral form demonstrated bathochromically shifted, vibronically resolved absorption bands peaked at 585 and 638 nm (with a shoulder at 550 nm)[29] (Fig. S22a, ESI;† compare also the spectra of their monomers in Fig. S23†). On applying anodic potentials (from −0.5 to 1.2 V for **P(CNPh-ETTE)** and from −0.2 to 1.2 V for **P(Py-ETTE)**), the main peaks of the neutral polymers disappear on the cost of growing polaronic and bipolaronic absorptions of the p-doped polymers in the near infrared (NIR) region.

Quantitatively, the CIE 1976 color coordinates ($L^*a^*b^*$) were measured to track the color changes in the SEC experiments (Fig. 8). In the neutral state (at −0.2 V), **P(CNPh-ETTE)** showed a purple color ($L^*a^*b^*$ = 35.7, 4.4, −2.5) and **P(Py-ETTE)** showed a sand-like brown color ($L^*a^*b^*$ = 39.6, 1.5, −1.4). When the potentials were raised to +(0.3–0.4) V for **P(CNPh-ETTE)** or +(0.5–0.6) V for **P(Py-ETTE)**, new absorption bands in the NIR region started to appear that corresponded to the formation of charge carriers (polarons and bipolarons) in the materials in accordance with the CV data described above. Further increase of the applied potential resulted in a decrease of the absorptions of the neutral polymers and progressive growth of polaronic and bipolaronic bands, which underwent hypsochromic shifts at higher potentials (polaronic band: 1100 → 790 nm and 1060 → 770 nm; bipolaronic band: ≥2000 → 1300 nm and ≥2000 → 1500 nm, for **P(CNPh-ETTE)** and **P(Py-ETTE)**, respectively; Fig. 8a and b). It should be noted that the polaronic state bands did not disappear (and their intensities were not decreased) even at a high applied potential of +1.2 V. This is contrasting with the SEC behavior of **P(Ph-ETTE)**, in which case the initially growing polaronic band was hypsochromically shifted (1070 → 870 nm) reaching the maximum intensity at +0.7 V, and then disappeared on the cost of continuing growth of a broad bipolaronic band at higher wavelengths (Fig. S22, ESI†).

This difference in SEC behavior and in polaronic band transformations for **P(Ph-ETTE)** and for polymers with electron-withdrawing groups (**P(CNPh-ETTE)** and **P(Py-ETTE)**) defines their different electrochromic properties. **P(Ph-ETTE)** showed a deep-blue to transparent EC transition from the neutral to fully oxidized state with $L^*a^*b^*$ evolution from (30.5, 3.9, −8.9) to (33.9, −4.0, −13.5). The presence of the polaronic band in the fully oxidized **P(CNPh-ETTE)** and **P(Py-ETTE)**, blue tail of which is extended to the visible region of the spectrum, led to different color changes. In the fully oxidized state (at +1.2 V), **P(CNPh-ETTE)** showed a pale grey-blue hue (max absorbance in the NIR is ~0.5, $L^*a^*b^*$ = 44.1, −2.4, 4.1) with residual absorption in the long wavelength visible region of the spectrum. **P(Py-ETTE)** showed the pale grey-green hue in the oxidized state (max. absorbance in the NIR is ~0.61, $L^*a^*b^*$ = 48.4, 3.1, 8.9), again with some residual long-wavelength absorption in the visible region.

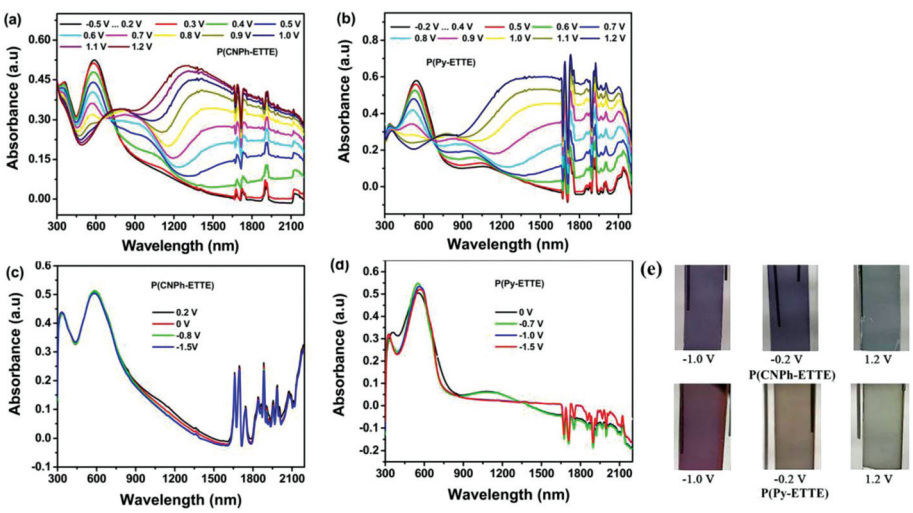

Fig. 8 Spectroelectrograms of polymer films deposited on ITO-coated glass slides in a monomer-free ACN/$TBAPF_6$ (0.1 M) solution: (a) **P(CNPh-ETTE)** between −0.5 and 1.2 V (oxidation); (b) **P(Py-ETTE)** between −0.2 and 1.2 V (oxidation); (c) **P(CNPh-ETTE)** at 0.2/0/−0.8/−1.5 V (reduction); (d) **P(Py-ETTE)** at 0/−0.7/−1.0/−1.5 V (reduction); (e) pictures of the films of **P(CNPh-ETTE)** (thickness 100 nm) and **P(Py-ETTE)** (thickness 105 nm) on ITO-coated glass slides at different potentials.

It is evident from Fig. 8a and b that at low positive or even at negative potentials (−0.5 to +0.2 V) there is a small amount of oxidation states in the neutral **P(CNPh-ETTE)** and **P(Py-ETTE)** polymers, which appear as weak polaronic absorptions in the NIR region. This is sometimes observed in EC conducting polymers when they cannot be fully dedoped from the trapped charges[56,57] and this is most likely caused by doping low-oxidation polymer films with atmospheric oxygen.[58] While electropolymerization was done under a nitrogen atmosphere, the SEC experiments in our setup were not performed *in situ* (the ITO slide with a polymer film was removed from the cell, washed, and then placed into the SEC cell of the spectrophotometer for measurements), so some oxidation/doping by an air might occur.

To check the possibility of full dedoping of the polymers and to verify whether the polymers have n-type behavior, we have performed SEC experiments at negative potentials. In the range of 0 to −0.7 V, the **P(Py-ETTE)** film still had a light-brown hue absorbing at λ_{max} ~ 545–550 nm and weak NIR absorption from trapped charge sites. Applying more negative potentials (−1.0 V or below) resulted in full dedoping of the polymer and disappearance of its polaronic band (Fig. 8d). This is accompanied by a minor bathochromic shift of the main band to λ_{max} = 560 nm and an irreversible color change to purple-red ($L^*a^*b^*$ = 42.4, 7.4, 3.1) (Fig. 8d and e). No further changes in spectra or film color were observed on applying more negative potentials down to −1.5 V. In contrast to **P(Py-ETTE)**, we were unable to fully dedope the **P(CNPh-ETTE)** polymer even at very negative potentials. At −1.5 V it still showed polaronic absorption as a tail to the neutral polymer band in the NIR region (~900–1400 nm) implying a small amount of deeply trapped charges (Fig. 8c). The color of the polymer film was the same at −0.2 and −1.0 V, and almost no spectral changes were observed in the visible and NIR regions from 0 to −1.5 V for this polymer (Fig. 8c and e).

The band gap estimated from the onset absorption of the fully dedoped **P(Py-ETTE)** at −1.0 V was found to be 1.72 eV,[59] *i.e.* somewhat lower than that for **P(Ph-ETTE)** (1.80 eV).[29] The band gap decrease of 0.08 eV is in good agreement with DFT calculations on these polymers (0.05 eV, Fig. 5). For **P(CNPh-ETTE)**, DFT predicts a slightly lower band gap (by 0.04 eV compared to **P(Py-ETTE)**). Its experimental determination from our SEC data (Fig. 8a) gave the value of 1.54 eV, *i.e.* substantially lower than that for **P(Py-ETTE)** and **P(Ph-ETTE)**. Although the decrease in the band gap from **P(Ph-ETTE)** to **P(CNPh-ETTE)** is expected and supported by DFT calculations, taking into account that we were unable to achieve full dedoping of **P(CNPh-ETTE)** (so, some polaronic absorption was still present in the polymer), one should take care with the accuracy of the given value, as the contraction of the band gap might be somewhat overestimated.[59] This is a common problem with estimation of the band gaps of conducting polymers with trapped charges from optical data, when full dedoping of the material cannot be achieved.[23] The electrochemical and optical properties of both **P(CNPh-ETTE)** and **P(Py-ETTE)** polymers are summarized in Table 1 and their CIELAB color coordinates are given in Table 2.

Electrochromic switching and the coloration efficiency

For deeper understanding of the electrochromic properties of the synthesized polymers, their optical contrast, coloration efficiency and response time were investigated by Vis-NIR spectroscopy (Table 2). The optical contrast of the polymers ΔT (*i.e.* the differences in transmittances between the neutral and oxi-

Table 1 Electrochemical and optical properties of the electrosynthesized polymers in films

Polymer	E^{ox}_{onset} (eV)	E^{red}_{onset} (eV)	λ_{max} (nm)	λ_{onset} (nm)	E_{HOMO} [a] (eV)	E_{LUMO} [b] (eV)	E_g^{opt} [c] (eV)
P(CNPh-ETTE)	0.09	−1.37	580	804[d]	−4.37	−2.83	1.54[d]
P(Py-ETTE)	0.83	−1.49	545	720[e]	−5.11	−3.39	1.72[e] (1.67)[59]
P(Ph-ETTE) [29]	0.07	—	585, 638	690	−4.35	−2.55	1.80

[a] $E_{HOMO} = -E^{ox}_{onset}$ [*vs.* Fc/Fc$^+$] + 4.8 (eV).[60] [b] $E_{LUMO} = (E_{HOMO} + E_g^{opt})$.[60] [c] $E_g^{opt} = 1240/\lambda_{onset}$, where λ_{onset} is obtained from the absorption edge of the polymers in their neutral state. [d] Estimated at applied potentials of −0.5 to +0.2 V, where full dedoping was not achieved, showing some polaronic absorption (Fig. S24, ESI). [e] Estimated at an applied potential of −1.0 V; at more positive potentials, full dedoping was not observed as evidenced by a small polaronic peak at *ca.* 1000 nm that gave lower E_g^{opt} estimations (Fig. S24, ESI).[59]

Table 2 CIE colorimetric data, optical contrast, coloration efficiency and response time of the electrosynthesized polymers in films

	CIE 1976 color space, $L^*/a^*/b^*$				Response time, s	
Polymer	Neutral state	Oxidized state	Optical contrast ΔT, % (λ, nm)[a]	Coloration efficiency CE, cm^2 C^{-1} (λ, nm)[a]	Oxidation (bleaching)	Reduction (coloring)
P(CNPh-ETTE)	35.7/4.4/−2.5	44.1/−2.4/4.1	23 (570), 62 (1500)	120 (570), 440 (1500)	0.90	0.34
P(Py-ETTE)	39.6/1.5/−1.4	48.4/3.1/8.9	16 (540), 50 (1500)	190 (540), 324 (1500)	1.10	0.35
P(Ph-ETTE) [29]	30.5/3.9/−8.9	33.9/−4.0/−13.5	71 (590), 60 (1500)	309 (590), 174 (1500)	1.80	1.10

[a] Wavelengths at which ΔT and CE have been measured are given in the parentheses.

dized states) was estimated at two wavelengths: at the main absorptions of the polymers in the visible region and at the absorption of bipolarons in the NIR region (570/1500 nm for **P(CNPh-ETTE)** and 540/1500 nm for **P(Py-ETTE)**, Fig. 9a and b). The switching studies were performed using a square wave potential step method with a residence time of 10 s, and the response time (defined as the time required to reach 90% of the full response) was calculated from chronoamperometry measurements (Fig. 9c and d). For **P(CNPh-ETTE)**, the optical contrast estimated by monitoring the transmittance difference between the neutral and oxidized states was 23% at 570 nm and 62% at 1500 nm, with the response times of 0.90 s for bleaching and 0.34 s for coloring. **P(Py-ETTE)** exhibited an optical transmittance contrast of 16% at 540 nm and 50% at 1500 nm, requiring 1.1 s for bleaching and 0.35 s for coloring. For both polymers, the response times are lower than that for the reference polymer **P(Ph-ETTE)** (1.80 s for bleaching and 1.10 s for coloring, Table 2 [29]). The favorably high optical contrasts for the studied polymers in the NIR region implies that the polymers might be promising candidates for potential applications, such as thermal emissivity applications.[61]

The coloration efficiency (CE) is an important parameter of electrochromic materials characterizing the changes in the optical densities of materials between the colored and bleached forms as a function of injected/ejected charges. We have estimated the CE values for the studied polymers in the visible and in the NIR region from the transmittance profiles of **P(CNPh-ETTE)** and **P(Py-ETTE)**, and compared them with the previously studied polymer **P(Ph-ETTE)** (Table 2). In the visible region, the CE of **P(CNPh-ETTE)** and **P(Py-ETTE)** are reasonably high (120 and 190 $cm^2\ C^{-1}$, respectively), comparable to that for a benchmark electrochromic polymer PEDOT (183 $cm^2\ C^{-1}$),[62] although they are lower than that for **P(Ph-ETTE)** (309 $cm^2\ C^{-1}$). However, in the NIR region the coloration efficiencies of **P(CNPh-ETTE)** and **P(Py-ETTE)** are substantially higher (440 and 324 $cm^2\ C^{-1}$, respectively), exceeding that of **P(Ph-ETTE)** (174 $cm^2\ C^{-1}$). For comparison the **P(EDOT-ETTE)** polymer showed a CE of 148 $cm^2\ C^{-1}$ (560 nm) and 235 $cm^2\ C^{-1}$ (1600 nm).[27] Related polymers of EDOT–X–EDOT type with an electron-deficient heterocyclic moiety X showed lower (or comparable) coloration efficiencies, *e.g.* for X = benzo-2,1,3-thiadiazole: 86 $cm^2\ C^{-1}$ (428 nm), 109 $cm^2\ C^{-1}$ (1100 nm),[60] X = pyrido-2,1,3-thiazole: 154 $cm^2\ C^{-1}$ (431 nm), 257 $cm^2\ C^{-1}$ (1337 nm),[60] X = pyrido-2,1,3-selanazole: 60 $cm^2\ C^{-1}$ (433 nm), 144 $cm^2\ C^{-1}$ (1200 nm),[52] X = *N*-alkylbenzotriazole (with an additional dialkoxythiophene moiety in the backbone): 236–335 $cm^2\ C^{-1}$ (584–590 nm), 339–426 $cm^2\ C^{-1}$ (1600 nm).[63]

Morphology of the electropolymerized films

The surface morphologies of the polymer films were probed using atomic force microscopy (AFM) and scanning electron microscopy (SEM). AFM measurements were performed in a glove box under a N_2 atmosphere. Fig. 10a and b show AFM images and Fig. 10b and d show SEM images, for **P(CNPh-ETTE)** and **P(Py-ETTE)**, respectively. The **P(Py-ETTE)** film has a homogeneous and flat surface covered with nanometer-scale round bulbs of about 200 nm with the RMS (root-mean-square) roughness of around 12.5 nm. The surface of **P(CNPh-ETTE)** shows rod-like objects displaying a network structure with the RMS roughness of around 32.7 nm. On a macro level, the **P(CNPh-ETTE)** film displays a quite rough and interconnected network forming a very porous polymer structure (Fig. S25, ESI†). Such a porous network structure facilitates

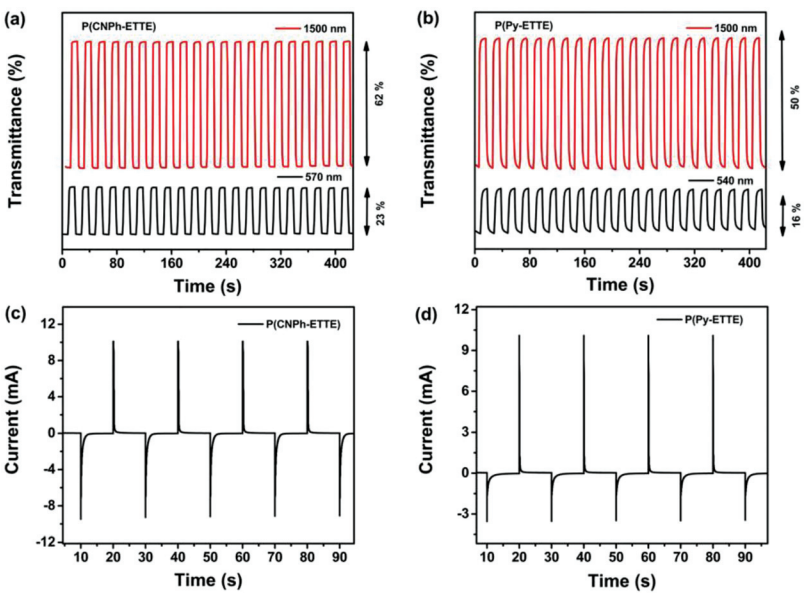

Fig. 9 Optical transmittance changes for polymer films on ITO-coated glass slides in ACN/$TBAPF_6$ (0.1 M): (a) **P(CNPh-EDOT)** at 570 and 1500 nm, (b) **P(Py-ETTE)** at 540 and 1500 nm. Chronoamperometry with a 10 s delay for each potential: (c) **P(CNPh-ETTE)** between −0.5 and 1.0 V; (d) **P(Py-ETTE)** between −0.2 and 1.2 V.

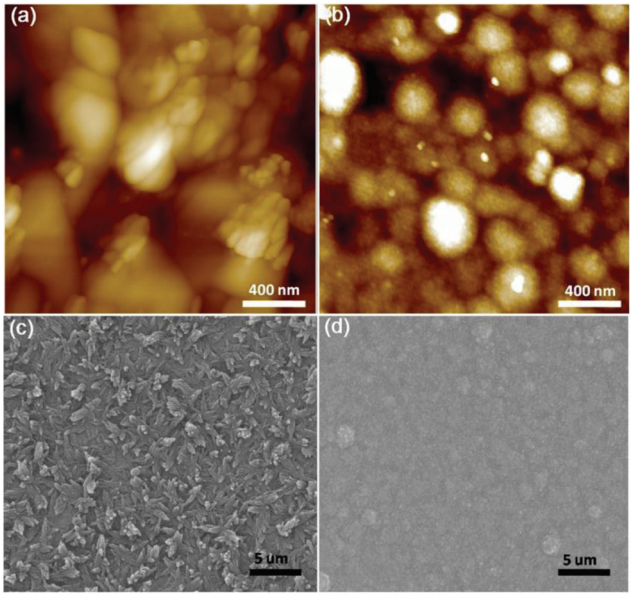

Fig. 10 AFM (a, b) and SEM (c, d; magnification of 25 000×) topography images of polymer films coated on ITO: (a, c) **P(CNPh-ETTE)**; (b, d) **P(Py-ETTE)**.

reversible doping/dedoping transformations that can explain the relative high stability and fast response time of this polymer.[64] Both RMS values are higher than in the reference polymer **P(Ph-ETTE)** (10.5 nm).[29]

Stability

The cycling life time is an important parameter for electrochromic applications. To explore the stability, the polymer films electrodeposited on the Pt electrode were swept repeatedly between the neutral and oxidized states using cyclic voltammetry in ACN/TBAPF$_6$ (0.1 M) at a scan rate of 150 mV s^{-1} under ambient conditions (Fig. 11). When scanned between −0.6 V and +1.2 V, the redox activity of the **P(CNPh-ETTE)** film remained 95% after 100 cycles and 75% after 1500 cycles (Fig. 11a) (the stability is estimated based on the peak current ratio). Under these conditions, the **P(Ph-ETTE)** film showed substantially poorer stability with a progressive decrease in the charge/discharge currents and it retained only 84% and 30% of its initial activity after 100 and 1000 cycles, respectively (Fig. 11c).

When **P(CNPh-ETTE)** and **P(Ph-ETTE)** are p-doped at a high applied potential of +1.2 V (Fig. 11a and c), the polymers are overoxidized, which might lead to an irreversible change in the polymer backbone.[65] It is known that overoxidation decreases the redox stability of conducting polymers. Therefore, we repeated the stability tests limiting the maximal applied potential just above the second oxidation peaks, at which full p-doping of **P(CNPh-ETTE)** and **P(Ph-ETTE)** is already observed. Cycling **P(CNPh-ETTE)** between −0.5 and +1.0 V demonstrated excellent stability of its p-doping/dedoping and the polymer retained over 90% of its electroactivity after 2000 cycles (96% and 91% as measured at the first and the second peak currents, j_{pa1} and j_{pa2}, respectively; 94–96% as measured by integration of either p-doping or p-doping/dedoping curves) (Fig. 11b). In the case of **P(Ph-ETTE)**, decreasing the potential range in cycling to 0.90/0.85/0.80 V also improved the redox stability of the polymer, but it was still substantially lower than that of **P(CNPh-ETTE)** (Fig. 11d and S26 in the ESI†). Thus, even when cycling to a maximum potential of V_{max} = 0.8 V (*i.e.* just above the second peak in CV), a pronounced decrease in the redox activity of **P(Ph-ETTE)** was observed remaining only 54% of its electroactivity after 2000 cycles.

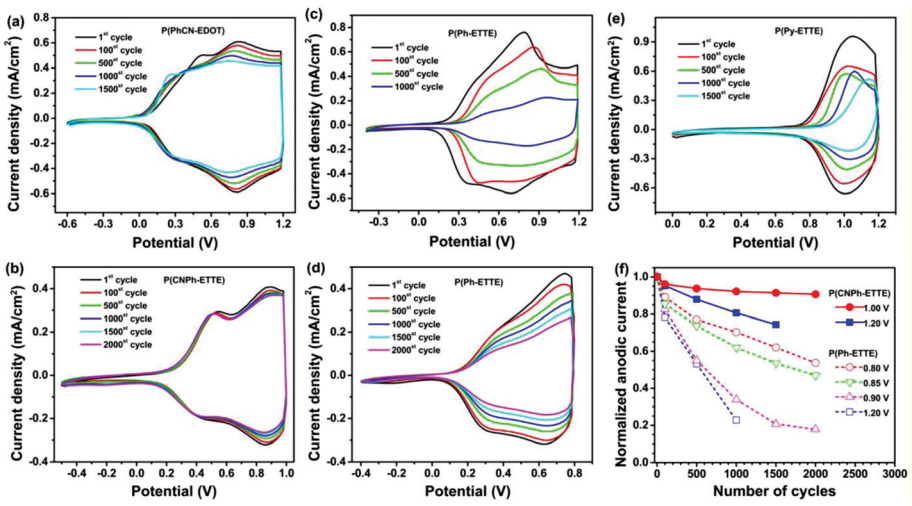

Fig. 11 Stability tests for polymer films on the Pt electrode using the CV method in a monomer-free ACN/TBAPF$_6$ (0.1 M) solution at 150 mV s^{-1} under ambient conditions: **P(CNPh-ETTE)**, cycled 1500 times between −0.6 and 1.2 V (a) and 2000 times between −0.5 and 1.0 V (b); **P(Ph-ETTE)**, cycled 1000 times between −0.4 and 1.2 V (c) and 2000 times between −0.4 and 0.8 V (d); **P(Py-ETTE)**, cycled 1500 times between 0 and 1.2 V (e). (f) Dependences of anodic current densities (shown in graphs (a–d) and in Fig. S26,† normalized to the maximum of the peak current j_{pa} at the 1st cycle) for **P(CNPh-ETTE)** and **P(Ph-ETTE)** *versus* number of cycles, tested at different potential ranges (maximal potentials are shown in the graph).

The differences in stabilities to p-doping/dedoping for **P(CNPh-ETTE)** and **P(Ph-ETTE)** are clearly seen from comparison of the evolution of the current densities at the maxima of their second oxidation waves (normalized to the peak currents at the first cycle) on cycling (Fig. 11f) that confirms the superior stability of **P(CNPh-ETTE)** over **P(Ph-ETTE)**. The reason for such a drastic difference between the structurally close polymers is not fully understood, and requires more detailed studies (possibly, with further variations in substituents at the phenyl ring of **P(Ar-ETTE)**), but we can speculate that it is related to the morphology of the films. From DFT calculations, the geometric and electronic structures of the isolated polymer chains for both polymers are quite close, therefore the electron-withdrawing effect of the side cyano groups on the polymer backbone is unlikely responsible for the observed differences. On the other hand, **P(CNPh-ETTE)** showed a more rough rod-like porous structure (Fig. 10a, c and S25a in the ESI†) compared to **P(Ph-ETTE)**.[29] For structurally related poly(3,4-phenylenedioxythiophene), PheDOT,[66] it was demonstrated that even small changes in the structure by functionalization of the monomer at the benzene ring lead to drastic changes in the electrodeposited films morphology and surface properties[67] (see also ref. 68). It is generally accepted that the polymer films with more open morphology, which provides a smaller diffusion distance for dopant ions, possess shorter switching times.[69] Thus, comparative studies on the stability of electrochromic poly(3,4-alkylenedioxythiophenes) showed that more porous morphology (by bulky substituents) reduces the number of trapped ion pairs after redox process cycling.[64] Very recently, Xu and co-workers have studied the long-term stability and the deterioration mechanism of electrochromic poly(3,4-(2,2-dimethylpropylenedioxy) thiophene), **PProDOT-Me2**, on redox cycling between the neutral and p-doped states.[70] Analysis of thin films of **PProDOT-Me2** by SEM and XPS revealed that the film morphology was changed from a loose irregular network to a compact structure with fibres covered by ions from the electrolyte (ClO_4^- and Li^+) as a result of chemisorption and physisorption during cycling. The adsorbed ions decreased the number of electroactive sites and blocked ion migration channels. Cross-section SEM images and XPS data indicated that trapped electrolyte ions cover the polymer surface more efficiently than inside the film, forming a compact structure and blocking the channels for the injection/ejection of ClO_4^- ions from the electrolyte, thus decreasing the lifetime of the EC material.

Relatively low charge/discharge stability was observed for the **P(Py-ETTE)** film, which possessed only 68% and 54% of electroactivity retained after 100 and 1500 cycles, respectively. Besides that, the anodic peak current of **P(Py-ETTE)** drifted seriously during the cycling process. The poor stability of the p-doped states of thiophene, selenophene and pyrrole copolymers with the pyridine moiety in the backbone has been reported previously.[50] We assume that the poor stability of **P(Py-ETTE)** is ascribed to the (partial) protonation of the pyridine rings of the polymer during cycling, which might cause deep trapping the charges and ions in the material and decrease its electroactivity.[64]

Conclusions

In conclusion, two novel electropolymerizable monomers based on the 2,5-(EDOT–TT–EDOT) motif, functionalized with electron-deficient 4-cyanophenyl and 4-pyridyl side groups in the positions 3,6- of the central TT moiety, **CNPh-ETTE** and **Py-ETTE**, have been successfully synthesized. Their electrochemical polymerization leads to electroactive, cathodically coloring electrochromic polymers **P(CNPh-ETTE)** and **P(Py-ETTE)**. Electron deficient side groups decrease the energies of both the HOMO and LUMO orbitals of the polymers (located on the main chain of the polymers) and their somewhat stronger influence on the LUMO results in a band gap contraction of the materials compared to the reference polymer with phenyl side groups, **P(Ph-ETTE)** (from 1.80 eV to 1.54–1.72 eV). In combination with different behaviors of the polaronic bands formed in the p-doping process of **P(CNPh-ETTE)** and **P(Py-ETTE)** compared to **P(Ph-ETTE)**, this define their different electrochromic behavior as demonstrated in spectroelectrochemical experiments. While **P(Ph-ETTE)** shows a deep-blue to transparent EC transition on p-doping, polymers with electron-deficient groups, **P(CNPh-ETTE)** and **P(Py-ETTE)**, demonstrate purple to pale grey-blue and sand brown to pale grey-green color changes. Both **P(CNPh-ETTE)** and **P(Py-ETTE)** demonstrate extremely short switch times of 0.9–1.1 s for bleaching and 0.34–0.35 s for coloring. They show a moderate contrast in the visible region (16–23% at the maxima of their absorption) and favorably good contrast in the NIR region of 50–62% (at 1500 nm). Both **P(CNPh-ETTE)** and **P(Py-ETTE)** show reasonably high coloration efficiencies in the visible region, at the maxima of their absorption (120 and 190 $cm^2\ C^{-1}$, respectively) and even higher CE in the NIR region (440 and 324 $cm^2\ C^{-1}$, respectively, at 1500 nm). Possible protonation of pyridine rings during the electropolymerization of **Py-ETTE** and on p-doping/dedoping cycling of **P(Py-ETTE)** decreases the quality of the polymer films and their stability as electrochromic materials on cycling. On the other hand, **P(CNPh-ETTE)** demonstrates superior stability of the color switch retaining 91–96% of its electroactivity after 2000 cycles between −0.5 and +1.0 V. n-Doping of the polymers results in irreversible color changes and degradations of the polymers. DFT calculations performed on these and related polymers with the EDOT–TT–EDOT motif gave some deeper insights into the structural effects of this class of EC polymers on their geometric and electronic structures, particularly on the effects of 3,6-substitution with different side groups. These computational data together with experimental studies on **P(CNPh-ETTE)** and **P(Py-ETTE)** broaden the vision on the design of new promising conjugated electrochromic polymers with tailored properties.

Acknowledgements

This work was financially supported by the Shenzhen Key Laboratory of Organic Optoelectromagnetic Functional

Materials of Shenzhen Science and Technology Plan (ZDSYS20140509094114164), the Shenzhen Peacock Program (KQTD2014062714543296), the Shenzhen Science and Technology Research Grant (JCYJ20140509093817690 and JCYJ20160331095335232), the Nanshan Innovation Agency Grant (no. KC2015ZDYF0016A), the Guangdong Key Research Project (no. 2014B090914003 and 2015B090914002), the Guangdong Talents Project, the National Basic Research Program of China (973 Program, no. 2015CB856505), the Natural Science Foundation of Guangdong Province (2014A030313800), and the Guangdong Academician Workstation (2013B090400016). IFP thanks the Santander Universities Research Mobility Award to support his visit to Shenzhen.

References

1 D. R. Rosseinsky and R. J. Mortimer, *Adv. Mater.*, 2001, **13**, 783–793.
2 M.-H. Yeh, L. Lin, P.-K. Yang and Z. L. Wang, *ACS Nano*, 2015, **9**, 4757–4765.
3 J. Remmele, D. E. Shen, T. Mustonen and N. Fruehauf, *ACS Appl. Mater. Interfaces*, 2015, **7**, 12001–12008.
4 G. Sonmez and H. B. Sonmez, *J. Mater. Chem.*, 2006, **16**, 2473–2477.
5 A. M. Osterholm, D. E. Shen, J. A. Kerszulis, R. H. Bulloch, M. Kuepfert, A. L. Dyer and J. R. Reynolds, *ACS Appl. Mater. Interfaces*, 2015, **7**, 1413–1421.
6 B. Karabay, L. C. Pekel and A. Cihaner, *Macromolecules*, 2015, **48**, 1352–1357.
7 (*a*) W. M. Kline, R. G. Lorenzini and G. A. Sotzing, *Color. Technol.*, 2014, **130**, 73–80; (*b*) H. Yu, S. Shao, L. Yan, H. Meng, Y. He, C. Yao, P. Xu, X. Zhang, W. Hu and W. Huang, *J. Mater. Chem. C*, 2016, **4**, 2269–2273.
8 P.-L. T. Boudreault, A. Najari and M. Leclerc, *Chem. Mater.*, 2011, **23**, 456–469.
9 J. Chen and Y. Cao, *Acc. Chem. Res.*, 2009, **42**, 1709–1718.
10 J. Mei and Z. Bao, *Chem. Mater.*, 2014, **26**, 604–615.
11 N. Stutzmann, R. H. Friend and H. Sirringhaus, *Science*, 2003, **299**, 1881–1884.
12 (*a*) D. F. Perepichka, I. F. Perepichka, H. Meng and F. Wudl, in *Organic Light-Emitting Materials and Devices*, ed. Z. Li and H. Meng, CRC Press, Boca Raton, FL, 2007, ch. 2, pp. 45–293; (*b*) A. C. Grimsdale, K. L. Chan, R. E. Martin, P. G. Jokisz and A. B. Holmes, *Chem. Rev.*, 2009, **109**, 897–1091; (*c*) I. F. Perepichka, D. F. Perepichka, H. Meng and F. Wudl, *Adv. Mater.*, 2005, **17**, 2281–2305.
13 L. Chen, B. Zhang, Y. Cheng, Z. Xie, L. Wang, X. Jing and F. Wang, *Adv. Funct. Mater.*, 2010, **20**, 3143–3153.
14 A. P. Kulkarni, C. J. Tonzola, A. Babel and S. A. Jenekhe, *Chem. Mater.*, 2004, **16**, 4556–4573.
15 H. Peng, L. Zhang, C. Soeller and J. Travas-Sejdic, *Biomaterials*, 2009, **30**, 2132–2148.
16 D. T. McQuade, A. E. Pullen and T. M. Swager, *Chem. Rev.*, 2000, **100**, 2537–2574.
17 C. M. Amb, A. L. Dyer and J. R. Reynolds, *Chem. Mater.*, 2011, **23**, 397–415.
18 M. Higuchi, Y. Akasaka, T. Ikeda, A. Hayashi and D. G. Kurth, *J. Inorg. Organomet. Polym. Mater.*, 2009, **19**, 74–78.
19 (*a*) I. McCulloch, M. Heeney, M. L. Chabinyc, D. DeLongchamp, R. J. Kline, M. Cölle, W. Duffy, D. Fischer, D. Gundlach, B. Hamadani, R. Hamilton, L. Richter, A. Salleo, M. Shkunov, D. Sparrowe, S. Tierney and W. Zhang, *Adv. Mater.*, 2009, **21**, 1091–1109; (*b*) P. J. Skabara, in *Handbook of Thiophene-Based Materials: Applications in Organic Electronics and Photonics*, ed. I. F. Perepichka and D. F. Perepichka, John Wiley & Sons, 2009, vol. 1, pp. 219–254.
20 M. E. Cinar and T. Ozturk, *Chem. Rev.*, 2015, **115**, 3036–3140.
21 W. T. Neo, Q. Ye, T. T. Lin, S. J. Chua and J. Xu, *Sol. Energy Mater. Sol. Cells*, 2015, **136**, 92–99.
22 E. Rustamlı, S. Goker, S. Tarkuc, Y. A. Udum and L. Toppare, *J. Electrochem. Soc.*, 2015, **162**, G75–G81.
23 L. Groenendaal, G. Zotti, P. H. Aubert, S. M. Waybright and J. R. Reynolds, *Adv. Mater.*, 2003, **15**, 855–879.
24 C. Kvarnström, H. Neugebauer, S. Blomquist, H. J. Ahonen, J. Kankare and A. Ivaska, *Electrochim. Acta*, 1999, **44**, 2739–2750.
25 J. Roncali, P. Blanchard and P. Frère, *J. Mater. Chem.*, 2005, **15**, 1589–1610.
26 G. J. McEntee, P. J. Skabara, F. Vilela, S. Tierney, I. D. W. Samuel, S. Gambino, S. J. Coles, M. B. Hursthouse, R. W. Harrington and W. Clegg, *Chem. Mater.*, 2010, **22**, 3000–3008.
27 X. Zhu, Y. Zhu, I. Murtaza, J. Shi, Y. He, P. Xu, M. Zhu, O. Goto and H. Meng, *RSC Adv.*, 2016, **6**, 75522–75529.
28 J. Shi, X. Zhu, P. Xu, M. Zhu, Y. Guo, Y. He, Z. Hu, I. Murtaza, H. Yu, L. Yan, O. Goto and H. Meng, *Macromol. Rapid Commun.*, 2016, **37**, 1344–1351.
29 P. Xu, I. Murtaza, J. Shi, M. Zhu, Y. He, H. Yu, O. Goto and H. Meng, *Polym. Chem.*, 2016, **7**, 5351–5356.
30 E. E. Havinga, W. ten Hoeve and H. Wynberg, *Synth. Met.*, 1993, **55–57**, 299–306.
31 L. Beverina, G. A. Pagani and M. Sassi, *Chem. Commun.*, 2014, **50**, 5413–5430.
32 Y. Sun, S.-C. Chien, H.-L. Yip, Y. Zhang, K.-S. Chen, D. F. Zeigler, F.-C. Chen, B. Lin and A. K. Y. Jen, *J. Mater. Chem.*, 2011, **21**, 13247–13255.
33 H. Zhou, L. Yang, S. C. Price, K. J. Knight and W. You, *Angew. Chem., Int. Ed.*, 2010, **49**, 7992–7995.
34 W. Li, L. Yan, H. Zhou and W. You, *Chem. Mater.*, 2015, **27**, 6470–6476.
35 M. Zhu, W. Li, P. Xu, J. Shi, S. Shao, X. Zhu, Y. Guo, Y. He, Z. Hu, H. Yu, Y. Zhu, I. F. Perepichka and H. Meng, *Sci. China: Chem.*, 2017, **60**, DOI: 10.1007/s11426-016-0305-9.
36 L. S. Fuller, B. Iddon and K. A. Smith, *J. Chem. Soc., Perkin Trans. 1*, 1997, 3465–3470.
37 S. M. Link, M. Scheuble, M. Goll, E. Muks, A. Ruff, A. Hoffmann, T. V. Richter, J. T. Lopez Navarrete,

M. C. Ruiz Delgado and S. Ludwigs, *Langmuir*, 2013, **29**, 15463–15473.

38 M. J. Frisch, G. W. Trucks, H. B. Schlegel, G. E. Scuseria, M. A. Robb, J. R. Cheeseman, G. Scalmani, V. Barone, B. Mennucci, G. A. Petersson, H. Nakatsuji, M. Caricato, X. Li, H. P. Hratchian, A. F. Izmaylov, J. Bloino, G. Zheng, J. L. Sonnenberg, M. Hada, M. Ehara, K. Toyota, R. Fukuda, J. Hasegawa, M. Ishida, T. Nakajima, Y. Honda, O. Kitao, H. Nakai, T. Vreven, J. A. Montgomery Jr., J. E. Peralta, F. Ogliaro, M. J. Bearpark, J. Heyd, E. N. Brothers, K. N. Kudin, V. N. Staroverov, R. Kobayashi, J. Normand, K. Raghavachari, A. P. Rendell, J. C. Burant, S. S. Iyengar, J. Tomasi, M. Cossi, N. Rega, N. J. Millam, M. Klene, J. E. Knox, J. B. Cross, V. Bakken, C. Adamo, J. Jaramillo, R. Gomperts, R. E. Stratmann, O. Yazyev, A. J. Austin, R. Cammi, C. Pomelli, J. W. Ochterski, R. L. Martin, K. Morokuma, V. G. Zakrzewski, G. A. Voth, P. Salvador, J. J. Dannenberg, S. Dapprich, A. D. Daniels, Ö. Farkas, J. B. Foresman, J. V. Ortiz, J. Cioslowski and D. J. Fox, *Gaussian 09, Revision A02*, Gaussian, Inc., Wallingford, CT, 2009.

39 (*a*) A. D. Becke, *Phys. Rev. A*, 1988, **38**, 3098–3100; (*b*) A. D. Becke, *J. Chem. Phys.*, 1993, **98**, 5648–5652.

40 C. Lee, W. Yang and R. G. Parr, *Phys. Rev. B: Condens. Matter*, 1988, **37**, 785–789.

41 E. Poverenov, Y. Sheynin, N. Zamoshchik, A. Patra, G. Leitus, I. F. Perepichka and M. Bendikov, *J. Mater. Chem.*, 2012, **22**, 14645–14655.

42 S. S. Zade, N. Zamoshchik and M. Bendikov, *Acc. Chem. Res.*, 2011, **44**, 14–24.

43 S. S. Zade and M. Bendikov, *Org. Lett.*, 2006, **8**, 5243–5246.

44 (*a*) M. Turbiez, P. Frère and J. Roncali, *J. Org. Chem.*, 2003, **68**, 5357–5360; (*b*) P. Leriche, M. Turbiez, V. Monroche, P. Frère, P. Blanchard, P. J. Skabara and J. Roncali, *Tetrahedron Lett.*, 2003, **44**, 649–652; (*c*) J.-M. Raimundo, P. Blanchard, P. Frère, N. Mercier, I. Ledoux-Rak, R. Hierle and J. Roncali, *Tetrahedron Lett.*, 2001, **42**, 1507–1510; (*d*) K. M. N. de Silva, E. Hwang, W. K. Serem, F. R. Fronczek, J. C. Garno and E. E. Nesterov, *ACS Appl. Mater. Interfaces*, 2012, **4**, 5430–5441.

45 M. Turbiez, P. Frère, M. Allain, C. Videlot, J. Ackermann and J. Roncali, *Chem. – Eur. J.*, 2005, **11**, 3742–3752.

46 J. Gierschner, J. Cornil and H.-J. Egelhaaf, *Adv. Mater.*, 2007, **19**, 173–191.

47 In a more precise approach, the band gap of a conjugated polymer (and in a similar fashion its HOMO and LUMO energy levels) can be expressed in terms of H. Kuhn's equation: $E_g = h^2(N+1)/8md^2(N+l)^2 + V_0(1-1/N)$, where h is Planck's constant, m is the electron mass, d is the averaged C–C and C=C bond lengths, N is the number of π-electrons, l is the effective length of the π-conjugated system, and V_0 is the constant corresponding to the band gap at infinite length: (*a*) H. Kuhn, *J. Chem. Phys.*, 1949, **17**, 1198–1212; (*b*) H. Kuhn and C. Kuhn, *Chem. Phys. Lett.*, 1993, **204**, 206–210; (*c*) G. Taubmann, *J. Chem. Educ.*, 1992, **69**, 96–97; (*d*) J. S. de Melo, L. M. Silva, L. G. Arnaut and R. S. Becker, *J. Chem. Phys.*, 1999, **111**, 5427–5433.

48 S. M. Link, M. Scheuble, M. Goll, E. Muks, A. Ruff, A. Hoffmann, T. V. Richter, J. T. Lopez Navarrete, M. C. Ruiz Delgado and S. Ludwigs, *Langmuir*, 2013, **29**, 15463–15473.

49 C. J. DuBois and J. R. Reynolds, *Adv. Mater.*, 2002, **14**, 1844–1846.

50 I. H. Jenkins, U. Salzner and P. G. Pickup, *Chem. Mater.*, 1996, **8**, 2444–2450.

51 D. J. Irvin, C. J. DuBois Jr. and J. R. Reynolds, *Chem. Commun.*, 1999, 2121–2122.

52 S. Ming, S. Zhen, X. Liu, K. Lin, H. Liu, Y. Zhao, B. Lu and J. Xu, *Polym. Chem.*, 2015, **6**, 8248–8258.

53 (*a*) B. Lu, S. Ming, K. Lin, S. Zhen, H. Liu, H. Gu, S. Chen, Y. Li, Z. Zhu and J. Xu, *New J. Chem.*, 2016, **40**, 8316–8323; (*b*) H. Zhao, D. Tang, J. Zhao, M. Wang and J. Dou, *RSC Adv.*, 2014, **4**, 61537–61547.

54 For the reduction processes, smaller peaks at *ca.* −(1–1.2) V are observed due to traces of an oxygen in the polymer films. This is particularly confirmed by minor peaks in the NIR region present in the dedoped polymers at −0.4/+0.2 V (see the Spectroelectrochemistry and colorimetry section).

55 J. A. Kerszulis, C. M. Amb, A. L. Dyer and J. R. Reynolds, *Macromolecules*, 2014, **47**, 5462–5469.

56 J. F. Mike, L. Shao, J.-W. Jeon and J. L. Lutkenhaus, *Macromolecules*, 2014, **47**, 79–88.

57 E. N. Esmer, S. Tarkuc, Y. A. Udum and L. Toppare, *Mater. Chem. Phys.*, 2011, **131**, 519–524.

58 K. Ogawa and S. C. Rasmussen, *Macromolecules*, 2006, **39**, 1771–1778.

59 Estimation of the E_g^{opt} for **P(Py-ETTE)** at −0.2 to +0.3 V where a minor polaronic band is still present, gave a lower value of 1.67 eV, underlying the uncertainty of the E_g^{opt} determination for not fully dedoped polymers and possible errors. One should be careful when using the literature data with the band gap estimations of partly doped polymers.

60 S. Ming, S. Zhen, K. Lin, L. Zhao, J. Xu and B. Lu, *ACS Appl. Mater. Interfaces*, 2015, **7**, 11089–11098.

61 T. T. Steckler, P. Henriksson, S. Mollinger, A. Lundin, A. Salleo and M. R. Andersson, *J. Am. Chem. Soc.*, 2014, **136**, 1190–1193.

62 C. L. Gaupp, D. M. Welsh, R. D. Rauh and J. R. Reynolds, *Chem. Mater.*, 2002, **14**, 3964–3970.

63 W. T. Neo, L. M. Loo, J. Song, X. Wang, C. M. Cho, H. S. O. Chan, Y. Zong and J. Xu, *Polym. Chem.*, 2013, **4**, 4663–4675.

64 J.-H. Huang, C.-Y. Hsu, C.-W. Hu, C.-W. Chu and K.-C. Ho, *ACS Appl. Mater. Interfaces*, 2010, **2**, 351–359.

65 S. A. Sapp, G. A. Sotzing and J. R. Reynolds, *Chem. Mater.*, 1998, **10**, 2101–2108.

66 (*a*) S. Roquet, P. Leriche, I. Perepichka, B. Jousselme, E. Levillain, P. Frère and J. Roncali, *J. Mater. Chem.*, 2004, **14**, 1396–1400; (*b*) I. F. Perepichka, S. Roquet, P. Leriche,

J.-M. Raimundo, P. Frère and J. Roncali, *Chem. – Eur. J.*, 2006, **12**, 2960–2966.

67 (*a*) C. R. Szczepanski, I. M'Jid, T. Darmanin, G. Godeau and F. Guittard, *J. Mater. Chem. A*, 2016, **4**, 17308–17323; (*b*) T. Darmanin, J.-P. Laugier, F. Orange and F. Guittard, *J. Colloid Interface Sci.*, 2016, **466**, 413–424.

68 T. Darmanin and F. Guittard, *Prog. Polym. Sci.*, 2014, **39**, 656–682.

69 (*a*) H. Yashima, M. Kobayashi, K. B. Lee, D. Chung, A. J. Heeger and F. Wudl, *J. Electrochem. Soc.*, 1987, **134**, 46–52; (*b*) A. A. Argun, P. H. Aubert, B. C. Thompson, I. Schwendeman, C. L. Gaupp, I. Hwang, N. J. Pinto, D. B. Tanner, A. G. MacDiarmid and J. R. Reynolds, *Chem. Mater.*, 2004, **16**, 4401–4412.

70 S. Guan, A. S. Elmezayyen, F. Zhang, J. Zheng and C. Xu, *J. Mater. Chem. C*, 2016, **4**, 4584–4591.